RETROGRADE WAVES IN THE COCHLEA

S. T. NEELY

Boys Town National Research Hospital,
Omaha, Nebraska 68131, USA
E-mail: neely@boystown.org

J. B. ALLEN

University of Illinois at Urbana-Champaign,
Urbana, Illinois 61801, USA
E-mail: jontalle@uiuc.edu

Retrograde waves in the cochlea are important because they provide information about cochlear mechanics that may be measured in the external ear canal as otoacoustic emissions. By extending traditional wave-variable methods, an explicit equation is derived for the forward-traveling wave in a one-dimensional cochlear model that is equivalent to the WKB approximation. The corresponding equation for the retrograde waves requires no additional approximation and provides a simple characterization of cochlear reflectance.

Keywords: cochlear model; wave propagation; reflectance; WKB.

1. Introduction

The importance of retrograde waves was not fully appreciated until the discovery of sounds measured in the ear canal that originate within the cochlea [1]. These otoacoustic emissions (OAE) provide a noninvasive means to acquire information about cochlear function.

Coherent reflection theory is the accepted explanation for stimulus-frequency OAEs (SFOAE) [2]. Zweig and Shera use the WKB approximation [3,4] to obtain a solution for the fluid pressure in a cochlear transmission line. Their *coherent reflection* theory provides a theoretical explanation for observed amplitude and phase characteristics of SFOAEs.

In this paper, wave-variable methods that have traditionally been applied to uniform transmission lines are extended to obtain the WKB formula described by [4]. This formulation leads to a simple equation for reflectance looking into the cochlea from the base.

2. Cochlear model

The equation for a one-dimensional long-wave transmission-line model of the cochlea[3] is

$$\frac{d}{dx}\begin{bmatrix} P(x,f) \\ U(x,f) \end{bmatrix} = -\begin{bmatrix} 0 & Z_s(x,s) \\ Y_b(x,s) & 0 \end{bmatrix}\begin{bmatrix} P(x,f) \\ U(x,f) \end{bmatrix}, \tag{1}$$

where $P(x,f)$ is the scala fluid pressure, $U(x,f)$ is the longitudinal volume velocity of the scala fluid, $Z_s(x,s)$ is the scala impedance (per unit length) and $Y_b(x,s)$ is the BM admittance (per unit length). The Laplace frequency s is used for expressions of frequency, such as impedances, that are causal functions in the time domain. The real frequency f (and $\omega \equiv 2\pi f$) are restricted to the Fourier transform of noncausal functions. These model variables are shown in Fig. 1 in the context of a single section of a transmission line.

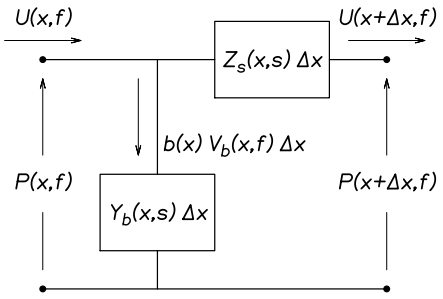

Fig. 1. Transmission line model for a section of the cochlea of length Δx. The series-impedance $Z_s(x,s)\Delta x$ limits fluid translational volume velocity $U(x,f)$, while the shunt-admittance $Y_b(x,s)\Delta x$ limits the basilar membrane volume velocity.

Scala impedance depends on fluid density ρ_0 and cross-sectional area $A(x)$.

$$Z_s(x,s) = s\rho_0/A_s(x). \tag{2}$$

BM velocity is proportional to the gradient of the scala volume velocity:

$$\frac{dU}{dx}(x,f) = -Y_b(x,s)\cdot P(x,f) = b\cdot V_b(x,f), \tag{3}$$

where b is the effective BM width.

3. Wave variables

The wave *propagation function* $\kappa(x,s)$ and the *characteristic impedance* $z_0(x,s)$ are determined entirely by the medium, and therefore only depend on the per unit length series impedance $Z(x,s)$ and shunt admittance $Y_b(x,s)$ [5]:

$$\kappa(x,s) \equiv \sqrt{Z_s(x,s)\cdot Y_b(x,s)} \tag{4}$$

$$z_0(x,s) \equiv \sqrt{Z_s(x,s)/Y_b(x,s)}. \tag{5}$$

The pressure *wave* variables P_+ and P_- are defined by

$$\begin{bmatrix} P_+ \\ P_- \end{bmatrix} \equiv \frac{1}{2}\begin{bmatrix} 1 & z_0 \\ 1 & -z_0 \end{bmatrix}\begin{bmatrix} P \\ U \end{bmatrix} \tag{6}$$

We invert Eq. 6

$$\begin{bmatrix} P \\ U \end{bmatrix} = \begin{bmatrix} 1 & 1 \\ y_0 & -y_0 \end{bmatrix}\begin{bmatrix} P_+ \\ P_- \end{bmatrix}, \tag{7}$$

where $y_0 = 1/z_0$, and substitute Eq. 7 into Eq. 1:

$$\frac{d}{dx}\begin{bmatrix} P_+ \\ P_- \end{bmatrix} = -\frac{1}{2}\begin{bmatrix} y_0 Z_s + z_0 Y_b + z_0 y' & -y_0 Z_s + z_0 Y_b - z_0 y' \\ y_0 Z_s - z_0 Y_b - z_0 y' & -y_0 Z_s - z_0 Y_b + z_0 y' \end{bmatrix}\begin{bmatrix} P_+ \\ P_- \end{bmatrix}. \tag{8}$$

In this equation $y_0' = dy_0/dx$. The equivalence of $y_0 Z_s = z_0 Y_b = \kappa$ allows Eq. 8 to be written as

$$\frac{d}{dx}\begin{bmatrix} P_+ \\ P_- \end{bmatrix} = \begin{bmatrix} -\kappa+\varepsilon & -\varepsilon \\ -\varepsilon & \kappa+\varepsilon \end{bmatrix}\begin{bmatrix} P_+ \\ P_- \end{bmatrix} \tag{9}$$

with

$$\varepsilon(x,f) \equiv \frac{1}{2}\frac{d}{dx}\ln z_0(x,s). \tag{10}$$

Note that when $z_0(x,s)$ is independent of x, ε is equal to zero, which decouples $P_+(x,f)$ and $P_-(x,f)$ in Eq. 9. When $z_0(x,s)$ varies slowly with x, $|\varepsilon/\kappa|$ is small, which may be exploited to obtain approximate model solutions.

Figure 2 shows examples of P_+ and P_- that demonstrate the importance of BM roughness in generating retrograde waves. Model parameters were selected to maintain nearly uniform characteristic impedance by making the scala area decrease with x at the same rate as BM stiffness [4]. The "tall broad peaks" of the BM excitation patterns were created by specifying a negative damping region at a location just basal to the tonotopic place. The negative damping was sufficient to boost the tip-to-tail ratio of the BM excitation patterns by about 60 dB. The model results shown in Fig. 2 were obtained by finite-difference solution of Eq. 1 and are called *exact* to contrast them with approximate results described below.

4. Approximate wave variables

The top row of Eq. 9 provides a differential equation for P_+ coupled to P_-

$$\frac{d}{dx}P_+ = (\varepsilon-\kappa)\,P_+ - \varepsilon P_-. \tag{11}$$

When $y_0(x,s)$ varies slowly with x, we can obtain an approximate equation for P_+ that is independent of P_- by assuming that $|(\kappa+\varepsilon)\,P_+| \gg |\varepsilon\,P_-|$. With this approximation, Eq. 11 reduces to

$$\frac{d}{dx}\widetilde{P}_+ = (\varepsilon-\kappa)\,\widetilde{P}_+ \tag{12}$$

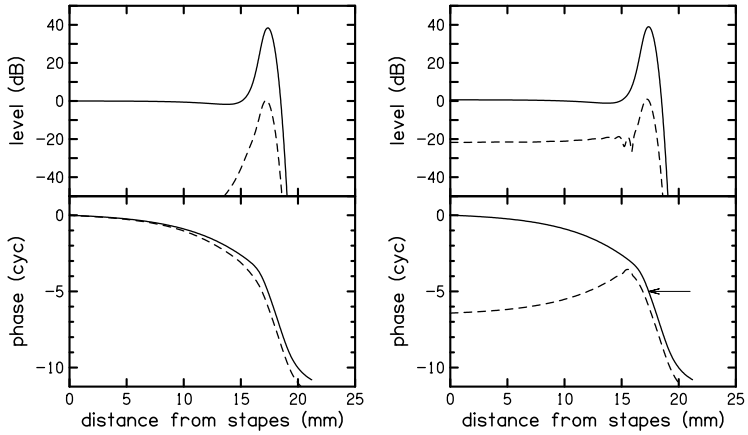

Fig. 2. Forward-traveling (solid) and retrograde (dashed) pressure components for the approximate model. The magnitude and phase are shown relative to pressure at the stapes. The results on the left side are for smooth BM impedance. The results on the right side are for rough BM impedance. The arrow indicates the phase at the characteristic place.

which can be integrated to obtain

$$\widetilde{P}_+(x,f) = P_+(0,f)\cdot\exp\left[\int_0^x \varepsilon(x_1,f)-\kappa(x_1,f)dx_1\right], \tag{13}$$

giving an approximate expression for P_+. Surprisingly this expression is the WKB approximation for the forward-traveling pressure wave [3,6,7].

The bottom row of Eq. 9 gives us a differential equation for P_- that is coupled to P_+,

$$\frac{d}{dx}P_- = (\kappa+\varepsilon)\,P_- - \varepsilon P_+. \tag{14}$$

No further approximations are needed to obtain a solution for the retrograde wave. Substitute Eq. 13 into Eq. 14 to obtain

$$\frac{d}{dx}\widetilde{P}_- - (\kappa+\varepsilon)\,\widetilde{P}_- = -\varepsilon P_+(0,f)\cdot\exp\left[-\int_0^x (\kappa-\varepsilon)\,dx_1\right]. \tag{15}$$

The integration of this equation requires a boundary condition. If we assume that $\widetilde{P}_-(L,f)\approx 0$, we obtain

$$\widetilde{P}_-(x,f) = P_+(0,f)\cdot\exp\left[\int_0^x (\kappa+\varepsilon)\,dx_1\right]\cdot\int_x^L \varepsilon\exp\left[-2\int_0^{x_2}\kappa dx_3\right]dx_2, \tag{16}$$

where x_2 and x_3 are additional integration variables for x. The sum of Eqs. 13 and 16 provides an approximate solution for the total pressure $\widetilde{P}(x,f)$. The accuracy of this approximation is demonstrated in Fig 3 by comparing exact and approximate solutions of peak pressure (at the characteristic place) relative to stapes pressure for versions of the cochlear model with smooth and rough BM. The exact solutions required about 20 times longer to compute.

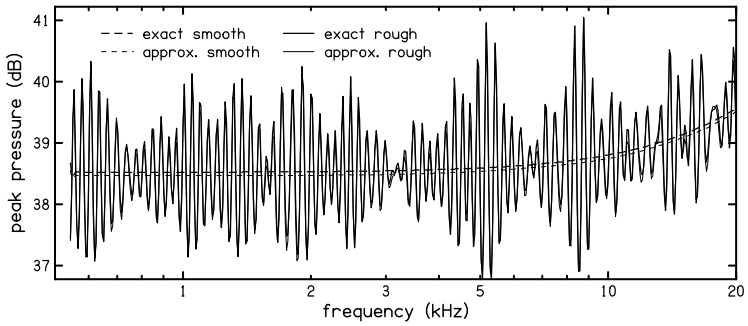

Fig. 3. *Peak pressure (re stapes pressure) as a function of frequency. The peak pressure is defined as the maximum pressure magnitude over the entire length of the BM at each frequency. The four curves represent different model conditions: (1) exact-smooth (thick dashed); (2) exact-rough (thick solid); (3) approximate-smooth (thin dashed); (4) approximate-rough (thin solid). The approximate results (thin) are barely visible in this figure because they are covered by the exact results (thick).*

We use Eqs. 13 and 16 to write an approximate equation for reflectance

$$\widetilde{\mathcal{R}}(x,f) = \exp\left[2\int_0^x \kappa(x_1)dx_1\right] \cdot \int_x^L \varepsilon(x_2)\exp\left[-2\int_0^{x_2} \kappa(x_3)dx_3\right] dx_2, \qquad (17)$$

which at the stapes reduces to

$$\widetilde{\mathcal{R}}(0,f) = \int_0^L \varepsilon(x_2)\exp\left[-2\int_0^{x_2} \kappa(x_3)dx_3\right] dx_2. \qquad (18)$$

Comparison between exact and approximate reflectance (not shown) demonstrate excellent agreement.

5. Discussion

Figure 2 shows exact model results for forward-traveling pressure P_+, and retrograde pressure P_-, at one frequency. The results on the left of Fig. 2 are for a smooth BM stiffness. The relatively small P_- level at the stapes indicates that reflection at the tonotopic place is insignificant. The results on the right are for a rough BM stiffness. The rough stiffness had a small, random increase added to the smooth stiffness at each place along the BM. The random stiffness increase was uniformly distributed between 0 and 0.001%. This small amount of roughness was sufficient to produce significant reflection of the forward-traveling wave in the vicinity of the tonotopic place. The positive slope of the phase of the P_- component indicates that retrograde energy is being propagated. Another interesting feature demonstated by the cochlear model results in Fig. 2 is that the round trip delay of an SFOAE may be less than the twice forward delay to the characteristic place.

In Fig. 3, we see that the pressure difference between the smooth and rough models (i.e., the peak pressure fine structure) is the same for the exact and approx-

imate results. In other words, the fine structure of the approximate pressure is the same as the fine structure of the exact pressure. Model peak-pressure fine structure represents *threshold* fine-structure rather than *SFOAE* fine-structure [8].

In Eq. 18, the accumulated phase of the incident wave $\widetilde{P}_+$ at location x comes primarily from the integral of κ. In Eq. 18, note that the contribution to the stapes reflectance $\widetilde{R}$ of the retrograde wave from any location x has twice the phase accumulation of the incident wave to that location. This doubling of phase is consistent with the mechanism of reflection being *place-fixed*. Experimental observations of OAE phase as a function of frequency suggest that some types of emissions are generated by a place-fixed mechanism [9].

6. Conclusions

The wave variable decomposition traditionally applied to uniform transmission lines may be extended to the case of nonuniform transmission lines, which may be used to represent one-dimensional models of cochlear mechanics. When the characteristic impedance z_0 varies slowly, the equations for $\widetilde{P}_+$, $\widetilde{P}_-$ and $\widetilde{\mathcal{R}}$ provide useful approximations for solutions of cochlear models with "tall broad peaks."

Acknowledgments

This work was partially supported by a grant from NIH-NIDCD (R01-DC8318).

References

1. Kemp, D., 1980. Stimulated acoustic emissions from within the human auditory system. J. Acoust. Soc. Am. 5, 1386-1391.
2. Zweig, G., Shera, C.A., 1995. The origin of periodicity in the spectrum of evoked otoacoustic emissions. J. Acoust. Soc. Am. 98, 2018-2047.
3. Zweig, G., Lipes, R., Pierce, J.R., 1976. The cochlear compromise. J. Acoust. Soc. Am. 59, 975-982.
4. Shera, C.A., Zweig, G., 1991. Reflection of retrograde waves within the cochlea. J. Acoust. Soc. Am. 89, 1290-1305.
5. Brillouin, L, 1953. Wave propagation in periodic structures. Dover, London, second edition.
6. Durney, C.H. Johnson, C.C., 1969. Introduction to modern electromagnetics. McGraw-Hill, New York.
7. Viergever, M.A., de Boer, E., 1987. Matching impedance of a nonuniform transmission line: Application to cochlear modeling. J. Acoust. Soc. Am. 81, 184-186.
8. Choi, Y.-S., Lee, S.-Y., Parham, K., Neely,S., Kim, D., 2008. Stimulus-frequency otoacoustic emission: Measurements in humans and simulations with an active cochlear model. J. Acoust. Soc. Am. 123, 2651-2669.
9. Shera, C.A., Guinan, J.J., 1999. Evoked otoacoustic emissions arise by two fundamentally different mechanisms: A taxonomy for mammalian OAEs. J. Acoust Soc. Am. 105 782-798.